mining

MDPI

Article

Numerical Model Validation with the Deformation Data from Intelligent Rock Bolts

Michel Varelija [1,*], Aleksandra Babaryka [1], Krzysztof Fulawka [2], Alexander Bondarchuk [3] and Philipp Hartlieb [1]

[1] Chair of Mining Engineering and Mineral Economics, University of Leoben, Erzherzog-Johann-Straße 3, 8700 Leoben, Austria; aleksandra.babaryka@unileoben.ac.at (A.B.); philipp.hartlieb@unileoben.ac.at (P.H.)
[2] KGHM CUPRUM Ltd. Research & Development Centre, Rock Engineering Department 2-8 gen., W. Sikorskiego Street, 53-659 Wrocław, Poland
[3] Boliden AB, Finnforsvägen 4, SE-936 81 Boliden, Sweden; alexander.bondarchuk@boliden.com
* Correspondence: michel.varelija@unileoben.ac.at

Abstract

Numerical modelling is a powerful tool used in geomechanics; however, its reliability depends on proper validation. This study demonstrates the use of intelligent rock bolt measurements to validate the numerical model of underground deformation, providing a practical and applicable approach even with all numerical modelling simplifications. A numerical model of a selected Case Study Location was developed using geomechanical data from laboratory tests (uniaxial compressive strength, triaxial test, and Brazilian test). The numerical model was validated using deformation data collected by intelligent rock bolts installed in the underground mine. Applying statistical data correction methods, the model data accuracy was further improved. Applying Kalman filtering improved the correlation between measured and modelled deformations from 0.90 to 0.98, demonstrating the effectiveness of statistical methods. The novelty of this work lies in the combined use of intelligent rock bolts, FEM simulations, and statistical data correction to achieve a practical and reproducible validation framework, even when simplified geological assumptions are used.

Keywords: intelligent rock bolts; numerical modelling; deformation measurement; mine digitalisation

1. Introduction

Underground mining is associated with geomechanical hazards, including roof collapses, rock bursts, and seismic activity, which pose serious risks to worker safety and operational continuity. Mining remains among the industries with the highest occupational risks [1], where rock mass instability can trigger costly reinforcement works, operational delays, and increased extraction costs [2]. To mitigate such risks, modern mines deploy a combination of preventive measures, including monitoring systems, optimised mine layouts, and improved support systems. Reliable methods for assessing geomechanical hazards are therefore essential for safe and efficient underground mining operations, particularly as global demand for minerals pushes extraction into deeper and increasingly complex geological conditions [3–5].

Check for updates

Academic Editor: Ali Mirzaghorbanali

Received: 2 July 2026
Revised: 7 August 2026
Accepted: 14 August 2026
Published: 19 August 2026

Copyright: © 2026 by the authors. Licensee MDPI, Basel, Switzerland. This article is an open access article distributed under the terms and conditions of the Creative Commons Attribution (CC BY) license.

Hazard prediction in underground mines can be approached using analytical, empirical, and numerical methods. Analytical and empirical methods enable rapid preliminary assessment but often have many simplifications in the calculation process. Artificial intelligence and neural networks have improved the handling of multi-parameter hazard prediction, integrating laboratory and in situ monitoring data [6,7]. However, such methods require extensive high-quality datasets, which are rarely available in active mine sites [8].

Numerical modelling remains a powerful tool for identifying potential instability zones and simulating excavation–rock mass interactions. Unlike purely analytical approaches, numerical models can integrate excavation geometry, variable rock properties, and dynamic loading conditions [9]. Nevertheless, conventional validation methods often rely on a single metric, which may not fully reflect the behaviour of underground structures. The key advantage of intelligent rock bolts lies in their ability to continuously capture real-time deformation data, providing a novel and more reliable basis for validating numerical models.

Conventional deformation monitoring techniques, such as extensometers, convergence meters, and strain gauges, have long been used to measure local displacements around underground excavations. However, these methods typically provide only discrete measurements at selected locations [10]. More recently, sensor technologies based on fibre-optic sensors are being used [11,12]. However, most of those methods provide only point or surface data measurements and require either a direct line of sight or complex installation procedures. Consequently, achieving continuous in situ deformation measurements within the rock mass itself remains a practical challenge.

Rock bolts with the function of measuring deformation are a suitable tool for validating numerical models because they can monitor deformations in the surroundings of workings as mining progresses [13]. However, the practical application of this approach is limited by the relatively low number of intelligent rock bolts installed in mining environments, largely due to their high cost. Increasing the density of instrumented rock bolts enhances the spatial representation of rock mass deformation, thereby improving the accuracy, resolution, and reliability of numerical model validation and predictive simulations.

While similar validation frameworks (i.e., numerical model results compared against measured deformation responses) have been applied in structural and civil engineering contexts (for example, in reinforced concrete beam modelling [14]) their application to underground rock mass environments and instrumented support systems remains scarce. This reflects both the practical challenges of installing and tracking in-rock deformation data in mining settings and the relative novelty of using in situ intelligent rock bolts for validation. Accordingly, the present work extends the model-validation paradigm into the underground mining domain, offering higher spatial resolution (more measuring instruments) and longer measurement duration than in previous research [15].

Hence, this study seeks to address the critical gap of deriving actionable insights from monitoring data by integrating it with simplified numerical modelling techniques, and subsequently applying this approach to a representative case study mine. This article demonstrates the process of numerical model validation using an innovative system for monitoring the deformation of underground excavations. The results of the six-month measurement campaign were compared to a numerical model based on data from laboratory tests. In subsequent computational iterations, the rock strength parameters were modified in a way that the simulation results and underground measurement results correlated properly. While the dataset is site-specific, the methodology is adaptable to other mining environments, providing a framework for model validation.

2. Literature Background on Numerical Model Validations

Numerical modelling is widely used in underground mining to evaluate excavation stability, simulate rock mass behaviour, and design safe extraction strategies. Commonly applied approaches include the finite element method (FEM), the finite difference method (FDM), and the discrete element method (DEM), each enabling a representation of excavation geometry, stress redistribution, and rock–support interactions under varying conditions. Despite their versatility, such models often rely on assumptions (like a homogeneous, elastic, isotropic material...), that may not fully reflect the complexity of in situ conditions. However, creating complex, detailed models is not very practical, as it requires a lot of detailed knowledge about the site conditions; thus, working with realistic expectations is an important aspect to consider. Monitoring systems provide field data necessary for model calibration and validation. Tools include convergometers, extensometers, and, most recently, intelligent rock bolts. Effective numerical model validation requires a combination of these monitoring and modelling tools to ensure reliable results. Various validation strategies have been proposed, ranging from calibration against historical instability events to iterative adjustment of rock mass parameters based on in situ deformation measurements. Numerical model validation involves comparing the model output to real-world data to ensure that predicted behaviour accurately represents the actual system.

Validation of the model on a laboratory scale is very effective while maintaining the appropriate level of model discretisation and maintaining the appropriate accuracy of the strength parameters of the analysed rock samples. The failure model on a laboratory scale can be successfully simulated in a 2D system, assuming appropriate boundary conditions and using an appropriate constitutive model [16–18].

In contrast, a large-scale model of underground areas presents greater challenges. In such a situation, the model calculated in the first iteration is most often characterised by large discrepancies from the real conditions in mines and must be validated. The validation can be performed in several ways; one most often used in the case of large-scale underground models is an attempt to adapt the stress distribution and the model's safety index to past cases of instability [19–21].

The validation method based on historical events is relatively simple to implement because it does not require performing a series of underground measurements. But from the point of view of prediction and the possibility of using numerical models to design safe and effective exploitation, such a method seems to be characterised by too low an accuracy. Moreover, an iterative approach to validating the numerical model can be carried out using a multi-point measurement of the convergence of underground workings [22]. The analysis covered a 10-month period during which the mining front progressed, affecting the state of deformation in the surroundings of the workings. Matching the results of underground measurements to the simulation results was achieved by reducing the strength parameters of the rocks based on the GSI scale, with the difference that the parameters of the GSI scale were reduced not based on the results of visual observation of the rock condition, but based on the results of simulated displacements, where the aim was to achieve maximum correlation with in situ recorded convergence values in subsequent months [22].

Figure 1 shows a satisfactory correlation level between the simulation and data, supporting the conclusion that a validated numerical model can be used as a tool for predicting geomechanical hazards. This statement is supported by the identification of areas of potential seismic activity that coincided with the actual locations of mining tremors. Despite the presented positive results, the accuracy of this approach was constrained by the limitations of the mechanical convergometers used for data acquisition [22].

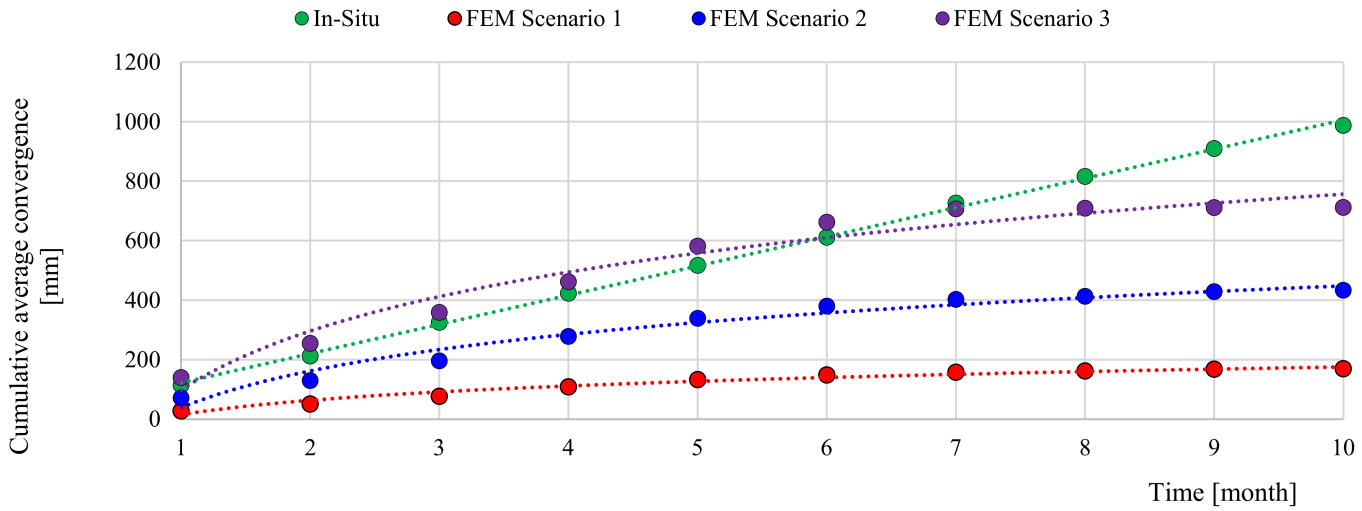


Figure 1. Comparison of average measured convergence with results of numerical simulations [22].

Building on these findings, the present study proposes the use of intelligent rock bolts to enable the high-resolution monitoring of underground excavation deformation. By providing continuous and precise deformation measurements, this system enables improved calibration of numerical models to in situ conditions, thereby enhancing their reliability for the design of safe and efficient mining operations.

3. Methodology

The methodology developed in this study contains the complete procedure, from the design and installation of intelligent rock (IR) bolts on-site to the acquisition, analysis and comparison of deformation data for model validation. This integrated approach enables the collection of high-resolution geotechnical data and its comparison with the numerical simulation output, thereby enhancing the precision of the entire process. The validation procedure ensures that the model represents in situ conditions as closely as possible, while incorporating necessary simplifications to optimise computational efficiency.

The selection and positioning of the IR bolts were determined in close collaboration with Boliden's mine management and planning team. Bolts were chosen for their dual capability to provide structural support while simultaneously monitoring deformation, making them well suited for the testing of this novel and emerging technology. Before installation, representative rock samples were collected for laboratory characterisation at the Laboratory for Rock Mechanics, Technical University of Leoben. The conducted tests included the triaxial compression test, uniaxial compressive strength (UCS) test, and Brazilian indirect tensile strength test.

Based on the geotechnical context, available data, and the required model complexity, finite element analysis (FEM) was selected as the most appropriate numerical method. Model development included the detailed point cloud scan of the selected mine section geometry, discretisation of the numerical model, the selection of a suitable failure criterion, and the definition of relevant boundary conditions.

Data acquisition from the IR bolts started on 21 June 2023. The excavation of the first stope began in early October 2023, coinciding with the first increase in recorded data. The acquired data were processed and visualised for comparison with simulation results. The validation process consisted of iteratively adjusting the model until convergence between simulated and measured deformations was achieved. The calibration process was repeated iteratively until the difference between the model predictions and the measured data was minimised. Kalman filtering was applied in the final stage to refine simulation outputs

and further improve performance. The methodology is demonstrated in Figure 2, which summarises the workflow for numerical model validation using deformation data from IR bolts.

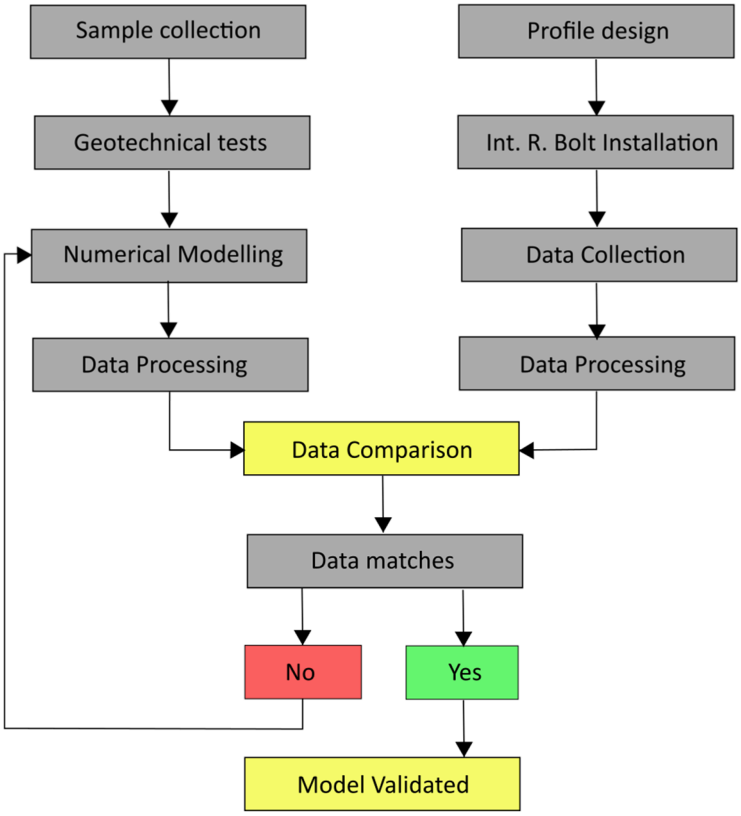


Figure 2. The workflow for the model validation from intelligent rock bolt deformation data.

3.1. Case Study Location—Boliden, Ravliden Mine

Boliden is a base metals producer operating in the smelters and mines business areas, with expertise spanning exploration, mining, mineral processing, smelting, sustainability, and metal recycling. To maintain underground safety, the company installs approximately 400,000 rock bolts annually.

The present study was conducted at the Rävliden mine, located 90 km west of Boliden town and approximately 750 km north of Stockholm, Sweden. The mine uses a long-hole stoping method to extract ore from volcanogenic massive sulphide deposits. This region is one of the most important mining districts in Sweden, producing copper (Cu), zinc (Zn), lead (Pb), silver (Ag), and gold (Au) [23]. The host rock at the monitoring site is mostly graphitic shale; a regional geological map (Figure 3) shows the distribution of major lithological units, providing geological context for the site.

Ground support at Rävliden follows a standard cycle of mechanical scaling, steel fibre-reinforced shotcrete (50 mm thickness), and systematic bolting in a 1.2 × 1.2 m pattern. The rock bolts are 20 mm in diameter, 2.7 m long, fully resin- or cement-grouted rebars, each fitted with a 100 × 100 × 10 mm face plate secured with a nut. Installation is carried out using Epiroc bolting machines.

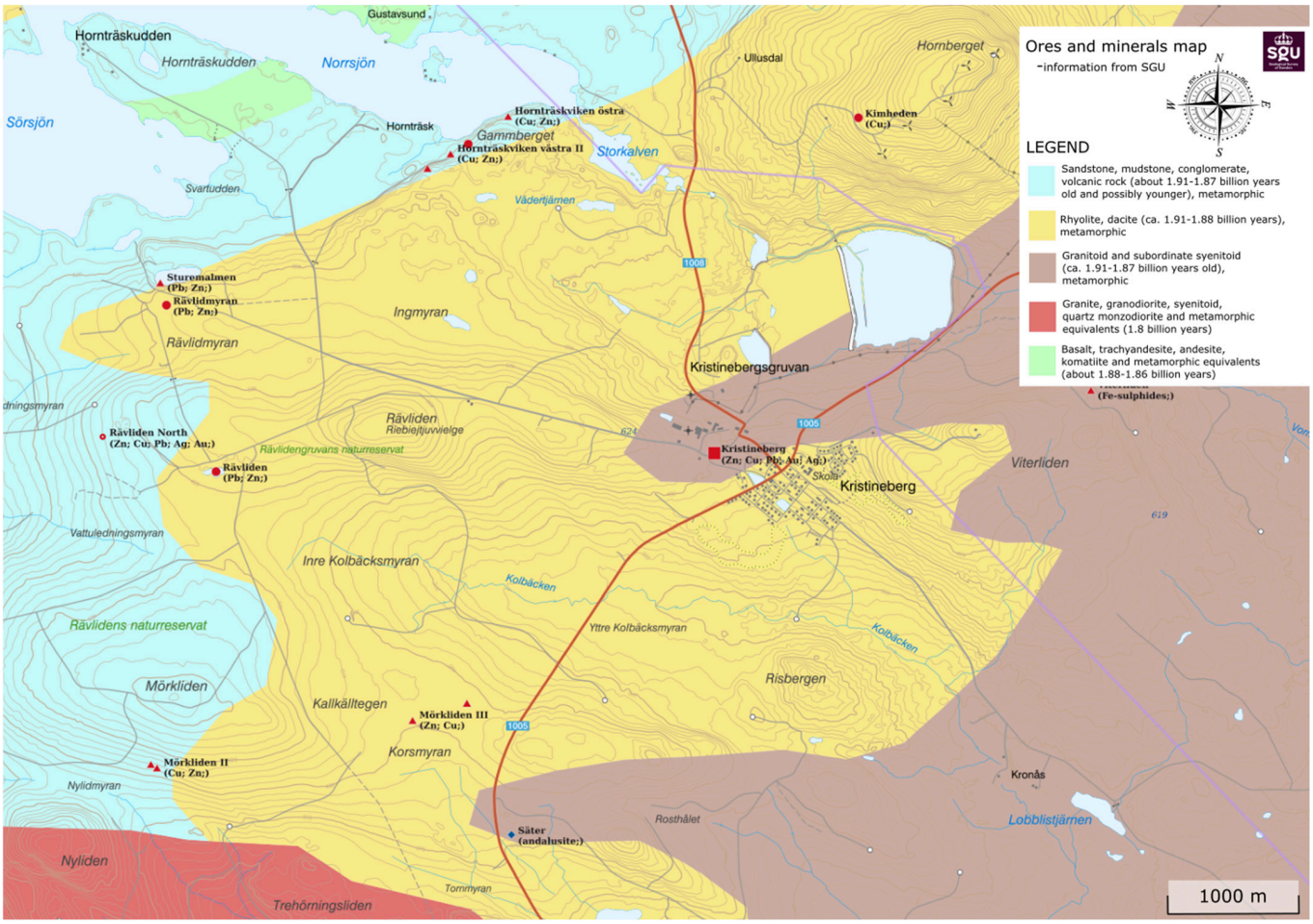


Figure 3. Geological map of the Rävliden area, showing the distribution of major lithological units [24].

3.2. Geotechnical Properties of Rävliden

The mechanical properties of the intact rock were determined by a testing programme that included the triaxial compression test, uniaxial compressive strength (UCS) tests under both stress-controlled and strain-controlled conditions, and the Brazilian tensile strength test. Table 1 summarises the laboratory test results as value ranges, reflecting the natural variability of the sampled material. Despite the controlled laboratory conditions, rock properties exhibited noticeable variation, representing the inherent heterogeneity of the rock mass. The rock mass in the mine can generally be described as competent and strong, with walls and the roof treated with shotcrete and showing no visible stability issues. The variability of the laboratory results presents a challenge for numerical modelling, as the complex behaviour of rock masses must be simplified into a limited set of representative parameters. For this study, a single representative value was selected for each property to enable the numerical modelling. However, this simplification inevitably reduces the level of detail, as it does not fully capture the entire range of variability observed in the tested material.

Table 1. Laboratory-derived mechanical properties of intact rock samples from the Rävliden mine. Reported values represent the range observed across all tested specimens, reflecting the inherent variability of the rock mass.

Parameter	Symbol	Unit	Lab Results Range
Young's Modulus	E	GPa	65–100

Table 1. *Cont.*

Parameter	Symbol	Unit	Lab Results Range
Cohesion	C	Mpa	20–50
Friction angle	ϕ	°	35–60
Poisson's ratio	v	-	0.10–0.20
Uniaxial compressive strength	σ_c	MPa	150–200
Tensile strength	σ_t	MPa	15–27

3.3. Monitoring

This section introduces the intelligent rock bolt monitoring technology and the installation layout used in this study. It describes the system capabilities and its potential application in underground mining, followed by a detailed explanation of the monitoring point selection, profile arrangement, and integration with the existing ground support pattern.

3.3.1. Intelligent Rock Bolts—Description and Capabilities

Intelligent rock bolts (IR bolts) are an emerging technology capable of measuring axial deformations while providing structural support [5,10]. By providing real-time data, IR bolts have the potential to improve the safety and reliability of underground structures. The advantages of intelligent rock bolts are numerous: they could reduce accidents, and improve the accuracy and precision of data collection and additionally, include additional sensors, for example, for continuous gas measurement. Using this comprehensive data, this system could send alerts to operators about changes in behaviour or when regular maintenance is required [25,26]. An intelligent rock bolt consists of several components, as shown in Figure 4. Along the steel bar is a sensor that records axial deformation at multiple points. The steel bar provides structural support, while a bolt nut secures it firmly against the bearing plate. The plate transfers the load from the bolt to the rock surface, ensuring anchoring. At the exposed end, a readout unit and a signal transmitter record the sensor data and transmit it wirelessly for storage and analysis [5].

Although the intelligent rock bolt records the deformation of the support element itself, the bolt is mechanically coupled with the surrounding rock mass and therefore responds to excavation-induced ground movement. Consequently, the measured deformation represents an indirect indicator of rock mass behaviours rather than a direct measurement of rock deformation. In this study, the measured bolt deformation was used to evaluate the agreement between observed and simulated deformation trends rather than to establish an exact equivalence between bolt and rock mass deformation.

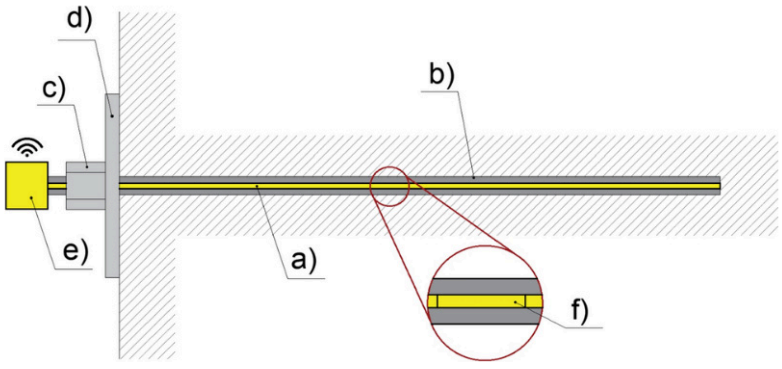


Figure 4. Intelligent rock bolt parts: (**a**) sensor along the steel bar, (**b**) rock bolt, (**c**) bolt nut, (**d**) plate, (**e**) readout unit and signal transmitter, and (**f**) one sensor segment [5].

3.3.2. Layout of the Intelligent Rock Bolts

The experimental model validation process described in this paper is novel and has not been implemented before. The site was carefully chosen in collaboration with Boliden, the mining company, focusing on a newly developed section of the mine that presented an ideal opportunity for real-time monitoring of rock mass behaviour. Furthermore, this location was selected due to the partnership between the research team and the mining company within the illuMINEtion project, which initiated the intelligent rock bolt monitoring system [27].

Due to the technology's testing phase, with logistical constraints and cost considerations, only a limited number of instruments were installed. This setup focused on monitoring a small section—specifically, a single top drift—rather than a full-scale installation across the entire mine. Three monitoring profiles were established strategically within the mine. The profiles are spaced approximately 20 m apart (Figure 5) to avoid redundancy while ensuring that key variations in deformation across the monitored section were recorded.

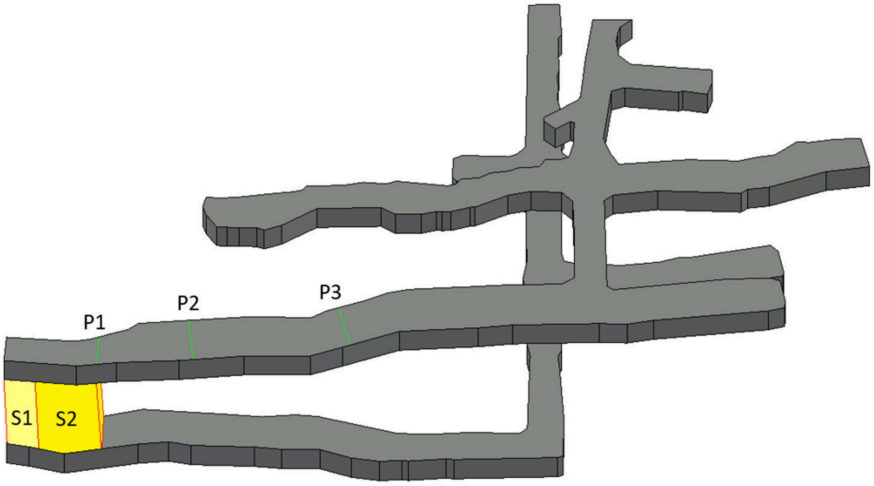


Figure 5. The model of the mine section, showing measurement profiles (P1–3) and stopes 1 and 2 (S1, S2).

Each profile is integrated into the mine's standard bolting pattern (Figure 6) and consists of three IR bolts: one installed in the roof and one in each sidewall. This arrangement was designed to capture deformation from multiple orientations. The IR bolts were configured to measure deformation every 30 min, a frequency deemed sufficient based on expected deformation rates.

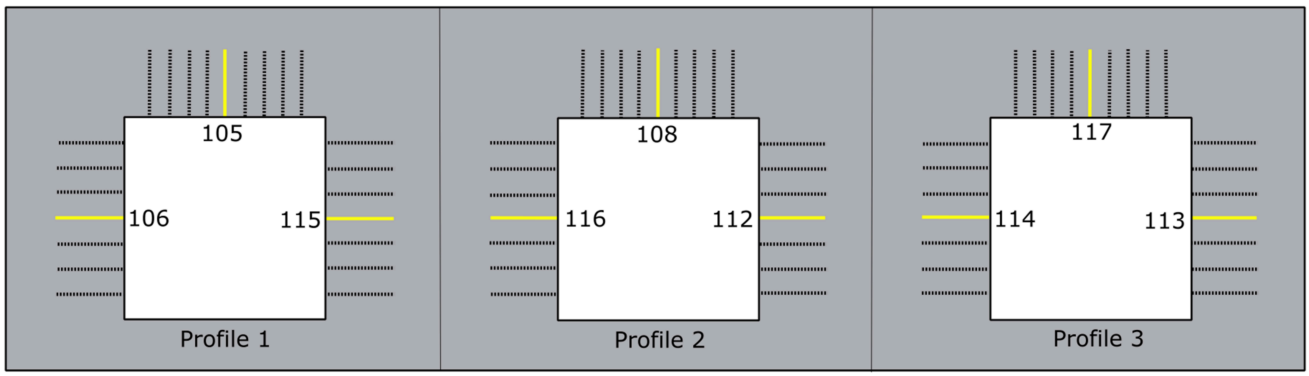


Figure 6. Layout of measuring Profiles 1–3, showing positions of intelligent rock bolts (yellow lines) with corresponding ID numbers and standard rock bolts (black dotted lines).

In summary, the dataset consists primarily of deformation measurements, providing valuable insights into the movement of the rock mass. The experimental nature of this approach, combined with the innovative technology used, offers a unique opportunity to monitor and analyse the behaviour of the rock mass response to stoping operations that has not been done before.

3.4. Numerical Model Setup

This section provides an overview of the numerical model setup, describing the components. It outlines the mining method sequence applied within the model, ensuring a clear understanding of the approach used throughout the analysis. The modelling software and numerical method selected are described, along with the geotechnical parameters used in the model, including rock mass properties, material strengths, and other relevant factors.

3.4.1. Modelled Mining Sequence of the Long Hole Stoping Method

The mining sequence modelled in this study directly reflects the actual mining operations carried out at the Rävliden site. By simulating the real-world excavation in stages, the model aims to closely represent the evolving ground conditions and rock mass behaviour throughout the mining process.

To ensure that the timing of support installation and excavation corresponded to the actual field activities, each stage in the model was aligned with the precise date and time when the respective mining operation was performed on-site. Since it is challenging to explicitly model continuous time-dependent behaviour in rock mechanics, the modelling approach focused instead on simulating distinct operational events. These included the top drift development, bottom drift development, the first stope excavation, and second stope excavation. By structuring the model around these discrete events, it was possible to capture the major geometrical and mechanical changes occurring in the rock mass during each mining phase, while maintaining a realistic correspondence with the actual mining sequence and support installation timeline. Figure 7 shows the geometry of the model in each stage of the mine section development:

Stage 1. Top Drift Development: The first step involves excavating the top drift. This drift is located according to the ore body, providing access for further development.
Stage 2. Bottom Drift Development: Once the top drift is established, the bottom drift is excavated. This drift is located below the top drift, and its development is important for the vertical extent of the ore body to be mined. Both drifts provide critical infrastructure for ventilation, access, and material transport during the next phases.
Stage 3. First Stope Excavation: With the top and bottom drifts in place, the first stope can be mined. The stope represents the primary area where ore is extracted. Careful planning is essential at this stage to ensure stability and efficient ore recovery, as well as to manage ground support.
Stage 4. Second Stope Excavation: After the first stope has been completed, mining proceeds to the second stope. This stope is adjacent to the first, and its excavation follows a similar process. The sequential extraction of these stopes ensures the structural integrity of the rock mass while optimising ore recovery.

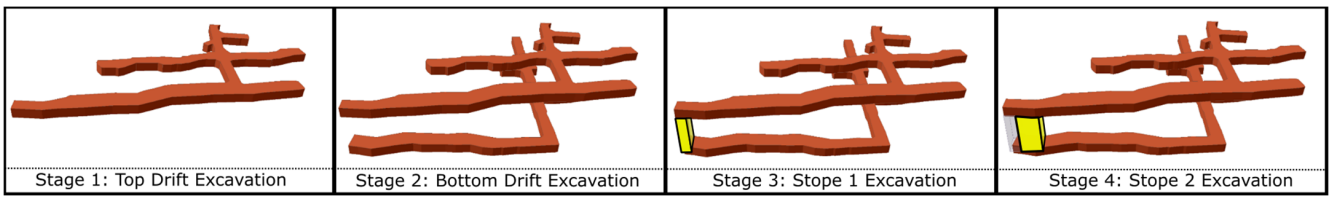


Figure 7. Stages of the simulated mining process.

Each stage in this sequence is carefully planned to balance safety, efficiency, and resource recovery, with continuous monitoring and adjustment to manage ground conditions and optimise production.

3.4.2. Used Software

Following the mining sequence described in the previous section, the excavation process was replicated numerically to capture its impact on the surrounding rock mass. This required a modelling tool capable of handling complex, moderately large geometries and sequential excavation steps. The numerical modelling in this study was carried out using RS3 (Rock and Soil 3D analysis programme, 2024 version, [28]). It is a specialised software for 3D modelling of underground excavations and open pits by using finite element analysis (FEM) for model computations.

FEM modelling is an element-based approach that is used for continuum mechanics. It was chosen as a suitable modelling technique, and it allows for the precise simulation of the linear-elastic behaviour of the rock mass based on the given parameters.

Although discontinuum methods such as DEM provide advantages for modelling explicit discontinuities, they generally require increased computational effort, particularly when detailed structures and iterative model evaluations are considered. Since the objective of this study was to investigate the feasibility of validating numerical deformation predictions using intelligent rock bolt measurements, FEM was selected as a suitable approach for representing the overall excavation response while maintaining computational efficiency.

3.4.3. Geotechnical Parameters Used in the Model

The initial parameter ranges used in the model were taken from laboratory tests on intact rock samples (Table 1). These values reflect the mechanical behaviour of the rock under controlled conditions but do not fully capture the complexities of in situ conditions. To improve the model's accuracy, the parameters were iteratively refined through a calibration process.

Initial values within the measured ranges were selected, the model was run, and the simulated displacements at selected points (Profiles 1–3, shown in Figure 6) were compared to those recorded by the intelligent rock bolts. When the results did not align with the measurements, the model was revisited and the parameters were adjusted—one at a time—until the combination that best matched the observed deformations was identified.

Through this step-by-step, trial-and-error process, the model was calibrated to represent not only the theoretical rock properties but also the actual ground response observed during excavation.

The final model simulates the elastic behaviour of the rock mass with the given parameters (Table 2).

Table 2. Geotechnical parameters used for the numerical model.

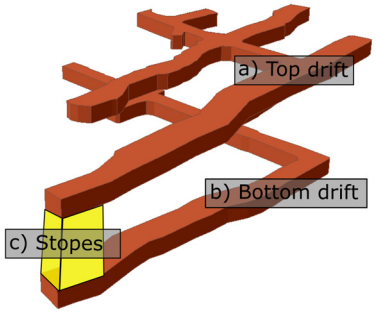
Parameter	Symbol	Unit	Model
Young's Modulus	E	GPa	65.0
Cohesion	C	Mpa	25.0
Friction angle	ϕ	°	40.0
Poisson's ratio	v	-	0.2
Tensile strength	σ_t	MPa	15.0

3.4.4. Geometry of the Model

The excavation geometry used in the numerical model is derived directly from a detailed point cloud of the monitored area, provided by Boliden. This point cloud captured the shape of the underground excavation with high spatial accuracy. The dataset was processed through a surface reconstruction workflow, in which the data was converted into a triangulated mesh (triangulated irregular network, TIN). This mesh represented the actual excavation surfaces and was subsequently imported into RS3, where it served as the basis for the solid geometry of the model. Using this method ensured that the model accurately reflected the true geometry of the top drift, bottom drift, and stope boundaries (Table 3).

Table 3. Average excavation dimensions, with a triangulated model.

Parameter	Axis	Dimension (m)
Top drift (a) width	X	6–10
Top drift (a) height	Z	6
Bottom drift (b) width	X	8–10
Bottom drift (b) height	Z	6
Stope (c) width	X	8–10
Stope (c) height	Z	20
Stope (c) length	Y	5



3.4.5. Incorporation of Site-Observed Geological Feature

During fieldwork for the installation of intelligent rock bolts, a distinct geological joint was observed intersecting two IR bolts in Profile 1. Its position and orientation were documented on-site. This joint was also evident in the deformation measurements, showing minimal movement before the stope extraction, but a slight increase in deformation afterwards. To capture this behaviour in the numerical model, a single joint element was implemented at the recorded position. While the exact mechanical properties of the joint were not available, its inclusion was based on field observations and deformation data patterns, ensuring that this key structural feature was represented in the simulation (Figure 8). The implementation aimed to reproduce the localised deformation increase associated with joint activation during stoping.

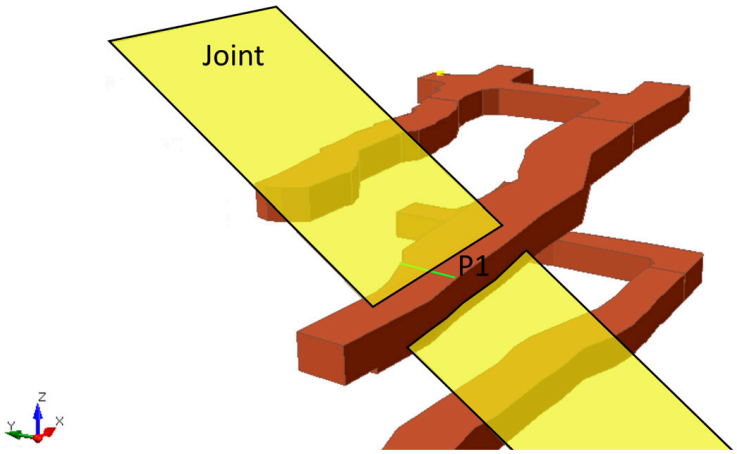


Figure 8. Joint position in the top drift.

3.4.6. Stress State

Vertical stress is induced by the gravity of a ground surface elevation of 750 m, and the unit weight of the overburden material is 24 kN/m^3. Horizontal stress is estimated by a k factor of 1.3 used for this model. This value was empirically derived by comparing deformation ratios between horizontal bolts installed in walls and vertical roof bolt deformations. Although the number of measurement points is limited, the model allows interpolation of data, providing a more detailed understanding of deformation patterns within the monitored section. Moreover, the initial horizontal stress coefficient was selected based on available regional information regarding in situ stress conditions. Due to the absence of direct stress measurements at the investigated location, the coefficient was subsequently refined through a comparison between numerical predictions and measured deformation responses. The calibrated value should therefore be interpreted as a case-specific parameter representing the stress conditions required to reproduce the observed deformation behaviour, rather than a direct measurement of the in situ stress state.

3.4.7. Numerical Model Mesh

The three-dimensional mesh was generated with the incorporated function within the RS3 software (2024 version) [28] via the built-in tetrahedral meshing algorithm. The software generates an unstructured tetrahedral grid that adapts to the model geometry and ensures the graded mesh is applied accordingly. The approach was adopted following the software guidelines for geotechnical analyses. Mesh quality is guaranteed within the RS3 software, ensuring that the element aspect ratios and transitions between zones are acceptable.

3.5. Data Processing and Model Validation Approach

The model validation process consisted of iteratively adjusting the model until convergence between simulated and measured deformations was achieved. In line with established practice, several correction strategies were employed to enhance model reliability, including parameter calibration and sensitivity-based adjustments. Where discrepancies persisted after parameter calibration, the iterative cycle was repeated, and in the final stage, a Kalman filter was applied to further refine the simulation outputs and improve agreement with field measurements.

3.5.1. Data Handling and Pre-Processing

The deformation data from the bolts were used in their raw form, without filtering, to preserve the integrity of the measurements. The only pre-processing involved calculating the total deformation for each bolt from the individual sensor readings along its length. Time alignment between the measured and simulated data was achieved using the installation timestamps recorded by the bolts and by modelling excavation stages in the FEM simulation according to the real mining sequence (Section 3.4.1). Data visualisation was carried out in the form of a time series for each monitoring profile.

3.5.2. Extraction of Model Outputs

The model was designed to match the geometry, excavation sequence, and bolt locations of the monitored mine section. Since the exact installation positions of the bolts were recorded during installation, these points were used as reference nodes in the numerical model. Deformation outputs were extracted from the model at these reference points, enabling direct spatial correspondence between the simulation and the measurement.

Additionally, as detailed in Section 3.4.4, a geological feature observed in the field was incorporated into the model. While full mechanical parameters were not available,

its location and orientation were based on direct site observations and confirmed through the measured deformation patterns. This ensured that an observed structural feature influencing local deformation was represented in the simulation.

3.5.3. Integration of Measured Data into Modelling

Integrating measured data into modelling requires compatible formats. Numerical modelling relies on measurable and estimated properties of rock masses, such as elastic modulus, Poisson's ratio, and/or joint systems etc. However, these data are typically obtained from laboratory experiments, which are costly to acquire at the density needed for accurate deformation analysis in mines. On the other hand, rock bolts provide direct deformation data that cannot be readily integrated into the simulation process. Instead, they can be used a posteriori to calibrate and adjust model predictions post hoc, thereby refining the predictions.

This adjustment can be performed using inverse modelling—which is inappropriate due to its high computational demands, often requiring hours to days of CPU time (e.g., 10–50 h on standard servers for large-scale rock mass models with thousands of parameters) and scaling poorly with the vast number of variables and data points in mine deformation analyses—or via statistical adjustment of the results, which is more efficient for real-time applications.

Building on validated measurements, numerical model predictions can be corrected post-simulation using real data to enhance accuracy. Data integration is complex when measurements and outputs misalign. In simple cases, apply mean or percentage adjustments. For complex structures like rock masses, use nonlinear or statistical methods—integrating regression, prior expertise, and physical models—for reliable estimates. Assess linear or polynomial regression fit (via mean/std against FEM data); if inadequate, employ advanced techniques. Integration of real-time data depends on the complexity of the case. In simple cases, linear regression substantially improves results. For more complex scenarios—such as larger datasets over extended periods—the Kalman filter is preferable, as it sequentially adjusts predictions based on prior measurements and associated errors [29].

To delve deeper, the following sections statistically analyse the correlation between FEMs and measured data. Kinematic models are then applied per literature recommendations, alongside Kalman filter integration. Finally, results are compared to evaluate the efficacy of these integrations.

4. Results

This chapter presents an overview of the results obtained from the study. It is divided into four parts: first, the raw deformation measurements collected by the intelligent rock bolts are presented and discussed; second, the results from the numerical model simulations are detailed; third, a comparison between the measured data and numerical predictions is provided to evaluate the model's fit; and finally, a statistical calibration of the model results is performed to refine and improve the fit between observed and simulated behaviour. Together, these sections offer a comprehensive understanding of the rock mass response during mining activities and the effectiveness of the modelling approach.

4.1. Measurement Results from the Intelligent Rock Bolts Installed On-Site

The deformation data collected from the intelligent rock bolts are visualised as time series, with each monitored profile containing measurements from three individual bolts. Figure 9 shows a top view of the monitored section, indicating the positions of Profiles 1–3 relative to the nearby drift.

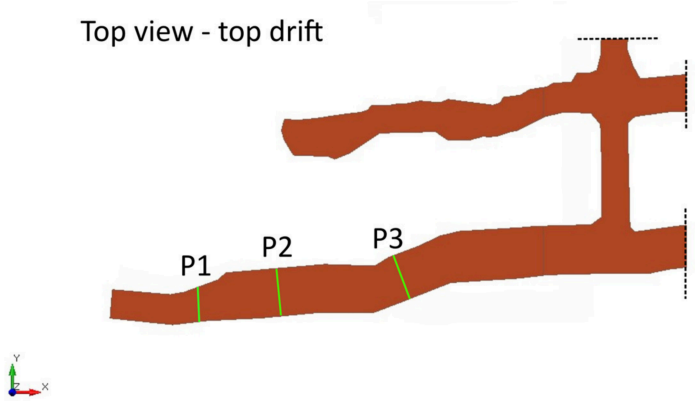


Figure 9. Top view of the monitored section, indicating the positions of Profiles 1–3 relative to the nearby drift.

The raw time-series data for each profile are presented in Figures 10–12. The following subchapters describe the measurements for each profile in detail. Each figure also includes the position of the profile within the section in the corner, providing spatial context for the measured deformations.

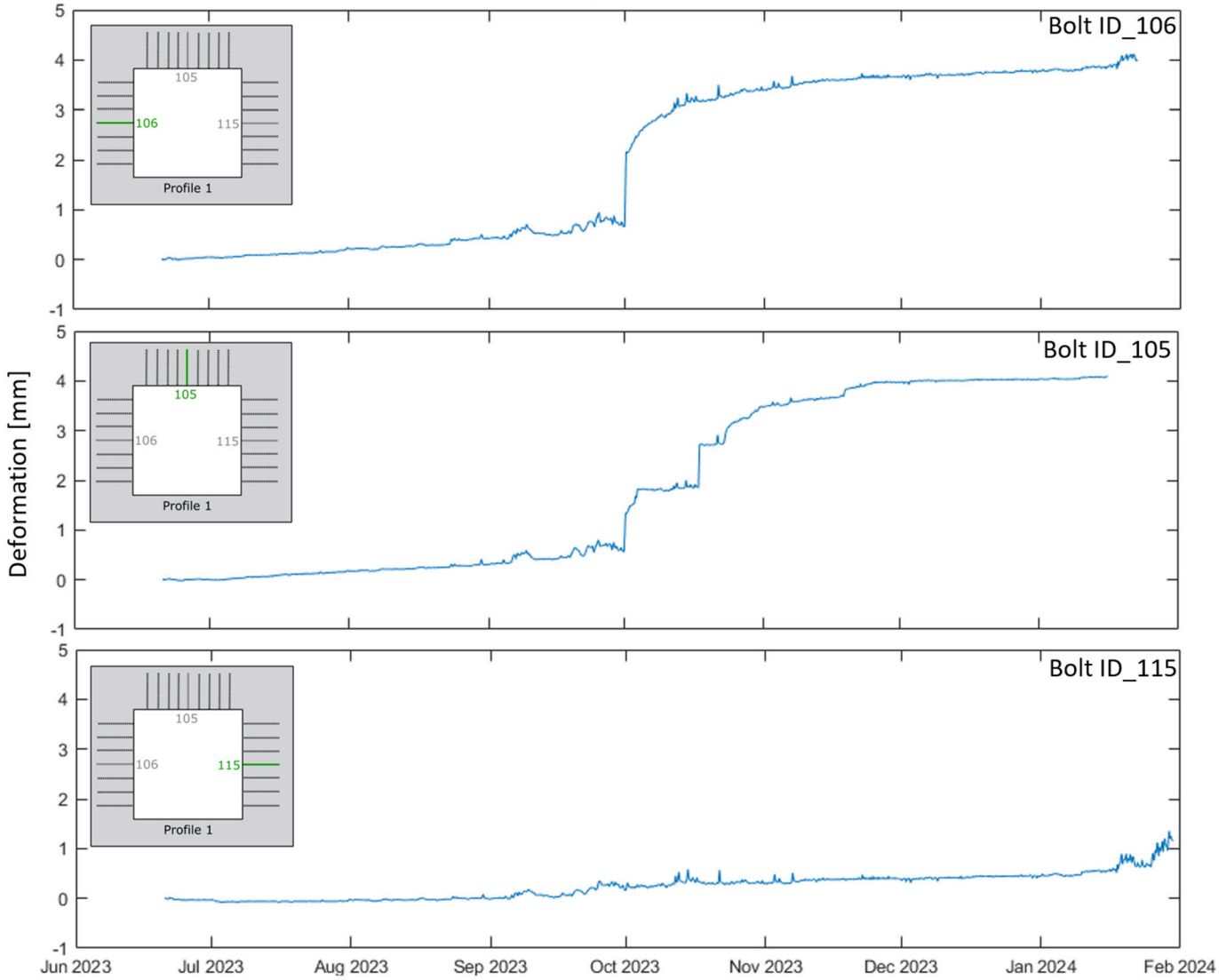


Figure 10. Time series of total deformation for Profile 1. Positions of the bolts within the profile are indicated in the left corner.

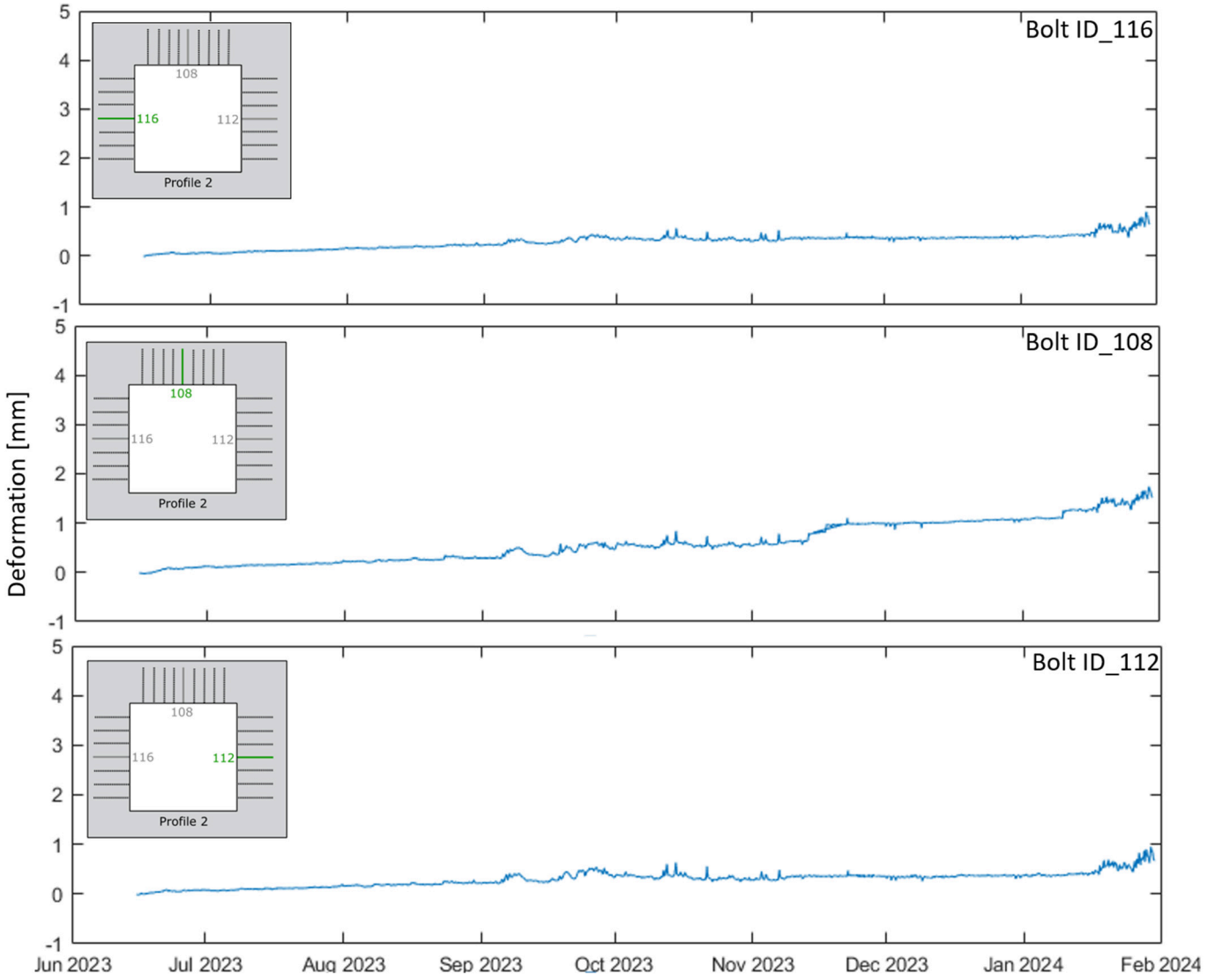


Figure 11. Time series of total deformation for Profile 2. Bolt positions are indicated in the left corner.

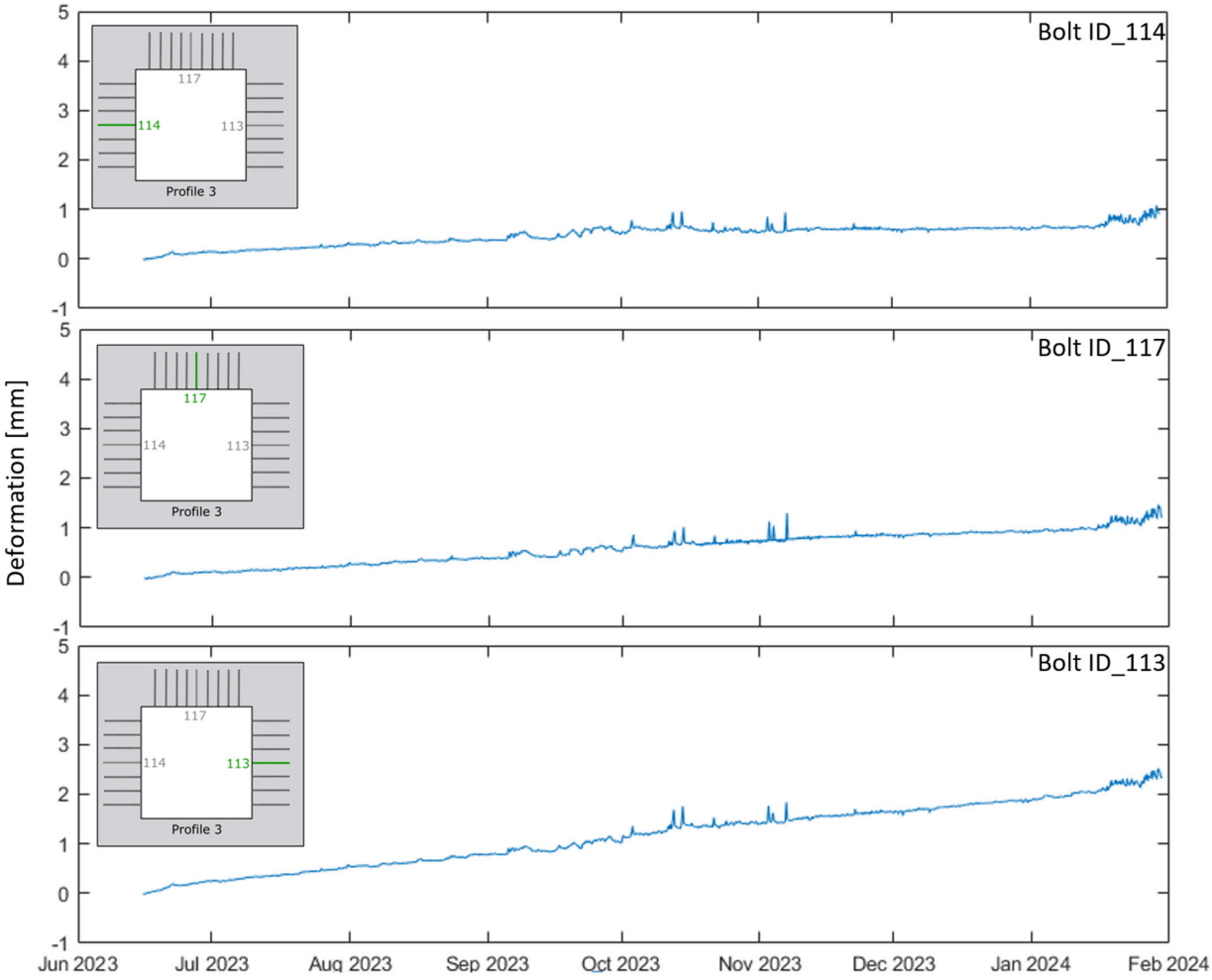


Figure 12. Time series of total deformation for Profile 3. Bolt positions are indicated in the left corner.

These results demonstrate how different parts of the same drift respond to excavation activities. The real-world deformation data gathered through intelligent rock bolts allowed for a demonstration of how proximity to mining operations affects rock mass behaviour. The contrasting results across the three profiles highlight the importance of location when assessing ground stability.

4.1.1. Profile 1

Profile 1 (Figure 10) recorded the highest deformations among the three measured profiles. This is consistent with expectations, as it is located closest to the stope development. The deformation data from Profile 1 clearly show increases in displacement as stope excavation progressed. The intelligent rock bolts in this area recorded continuous deformation, offering a direct correlation between excavation activities and rock mass response.

Notably, bolts 106 and 105 exhibit a marked increase in deformation immediately following the excavation of the first stope, which confirms the presence of the observed joint. In contrast, bolt 115 does not show this increase, providing insight into the joint's position. The fact that the joint deformation coincides with the stope excavation indicates it was activated by mining activity, although it was already visible on the wall during fieldwork. The second increase in the deformation in bolt 105 coincides with excavation of the second stope.

4.1.2. Profile 2

Profile 2 (Figure 11) exhibited the least deformation. As it is situated further from the stope and relatively unaffected by the nearby drift, the measurements indicate minimal rock mass movement. The three bolts in this profile show only slight changes over time, suggesting that this section remains stable despite ongoing mining operations.

4.1.3. Profile 3

Profile 3 (Figure 12) showed moderate deformation, with bolt number 113 recording the most notable increases, particularly in the sidewalls adjacent to a nearby drift. These localised deformations highlight the influence of underground openings on rock mass behaviour. The variation among the three bolts in this profile demonstrates how drift proximity can create heterogeneous deformation patterns.

4.2. Numerical Model Results

The numerical model was developed to replicate the excavation sequence, geometry, and bolt positions of the monitored mine section. To account for the fact that the intelligent rock bolts were installed after some excavation and support had already taken place, a correction was applied to the simulated data. Specifically, deformations that occurred before bolt installation were subtracted from the model results. Without this correction, the numerical model—which tracks deformation from the very start of excavation—would naturally produce larger values than those recorded in the field. In reality, rock mass movement begins immediately after excavation, with an inevitable short period during which the surrounding rock remains unsupported, resulting in initial settlement. In this case, the bolts were installed after excavation and support installation; therefore, this initial movement was not captured by the monitoring system. In contrast, in the numerical simulation, bolts are effectively "installed" immediately after excavation, which omits this unsupported period. To approximate real conditions, the model was executed in discrete steps to allow for preliminary settlement, though reproducing the exact timing of installation remained challenging. Preliminary tape measurements taken shortly after excavation provided reference values for this settlement.

After applying this correction, the simulated deformations matched the order of magnitude observed in the measurements. Figure 13 shows the modelled deformation pattern, with the bolt array clearly visible and the legend indicating deformation in metres.

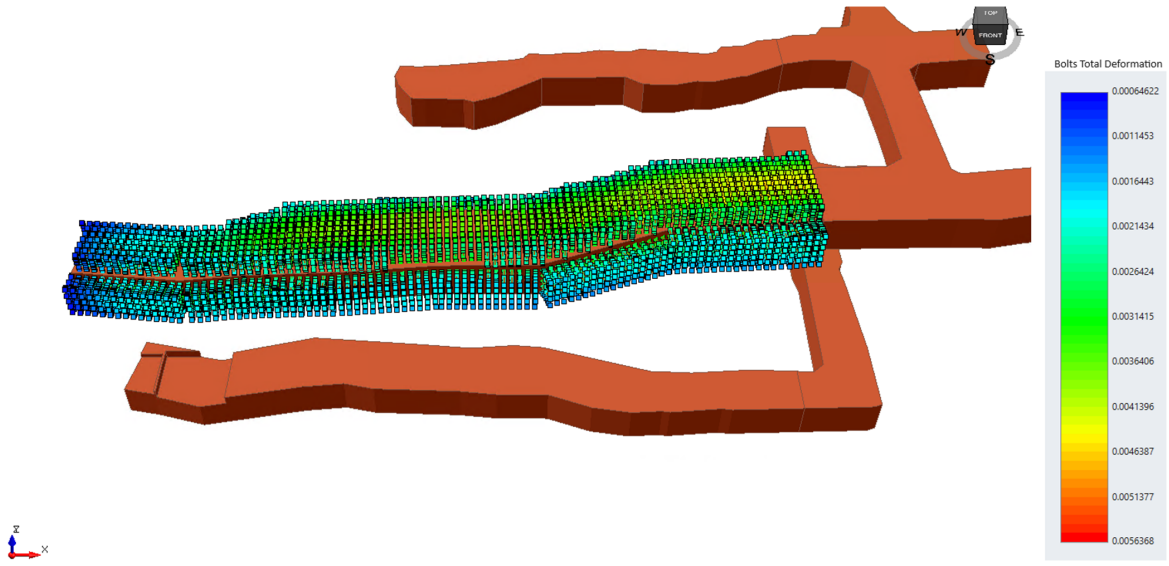


Figure 13. Result of the numerical model.

4.3. Comparison of Measurement Data and Numerical Model Results

Specific data points from the simulated results and real measurements are compared. Figures 14–16 show the differences between the measurements and simulations for Profiles 1–3. In the graphs, the same colour represents the same bolt, with dotted lines indicating the simulation results and solid lines representing the actual measurements. Intermediate points have been linearised for easier comparison. The trend observed in the graphs indicates that the model data follows the behaviour of the real measurements, capturing general deformation patterns.

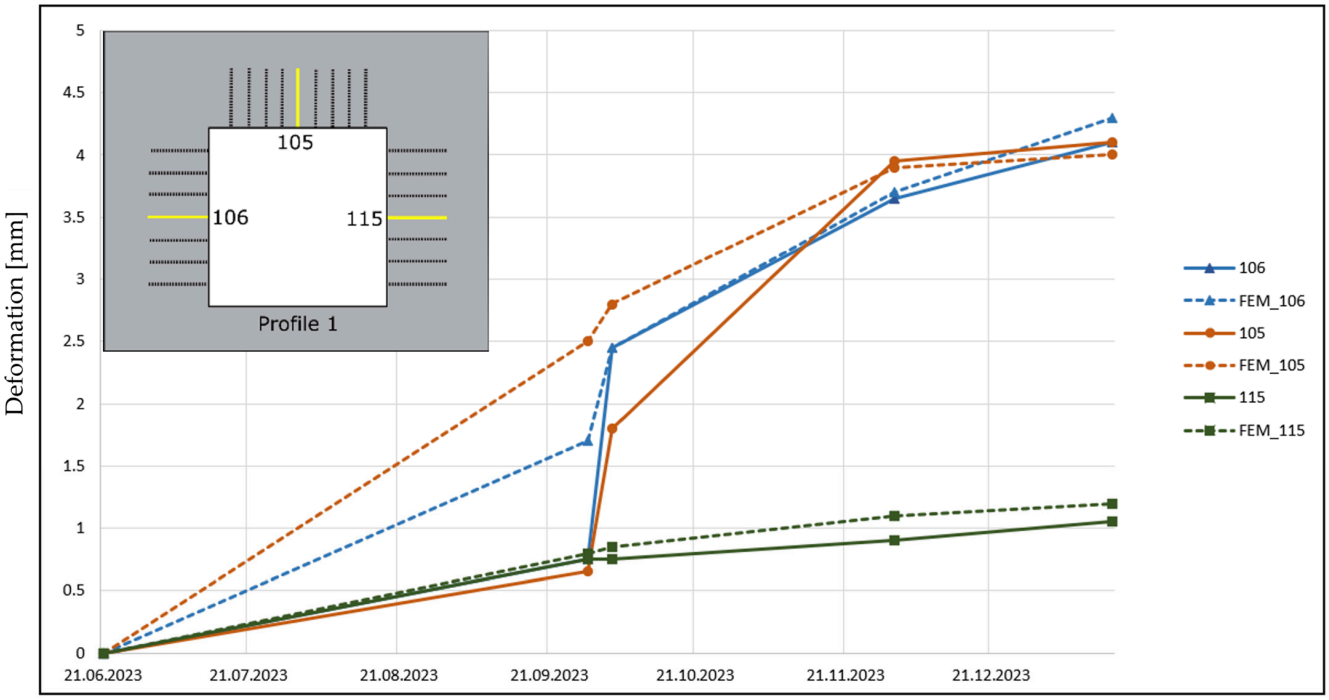


Figure 14. Data comparison—real measurements and simulated data (Profile 1).

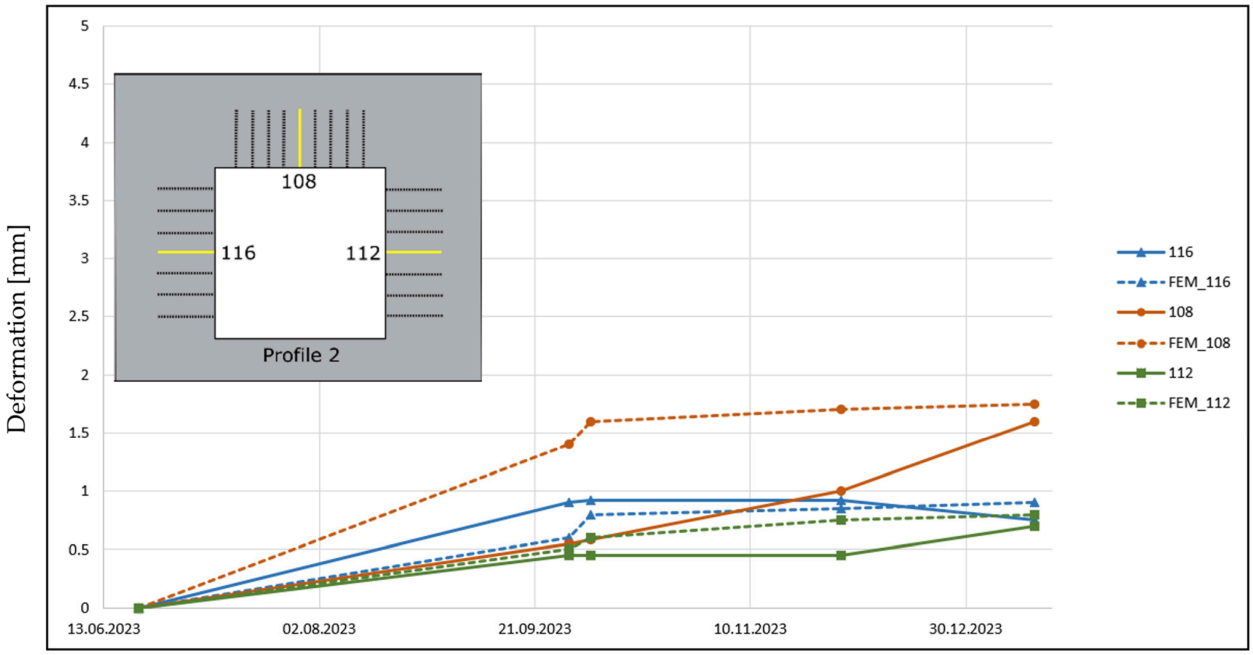


Figure 15. Data comparison: real measurements and simulated data (Profile 2).

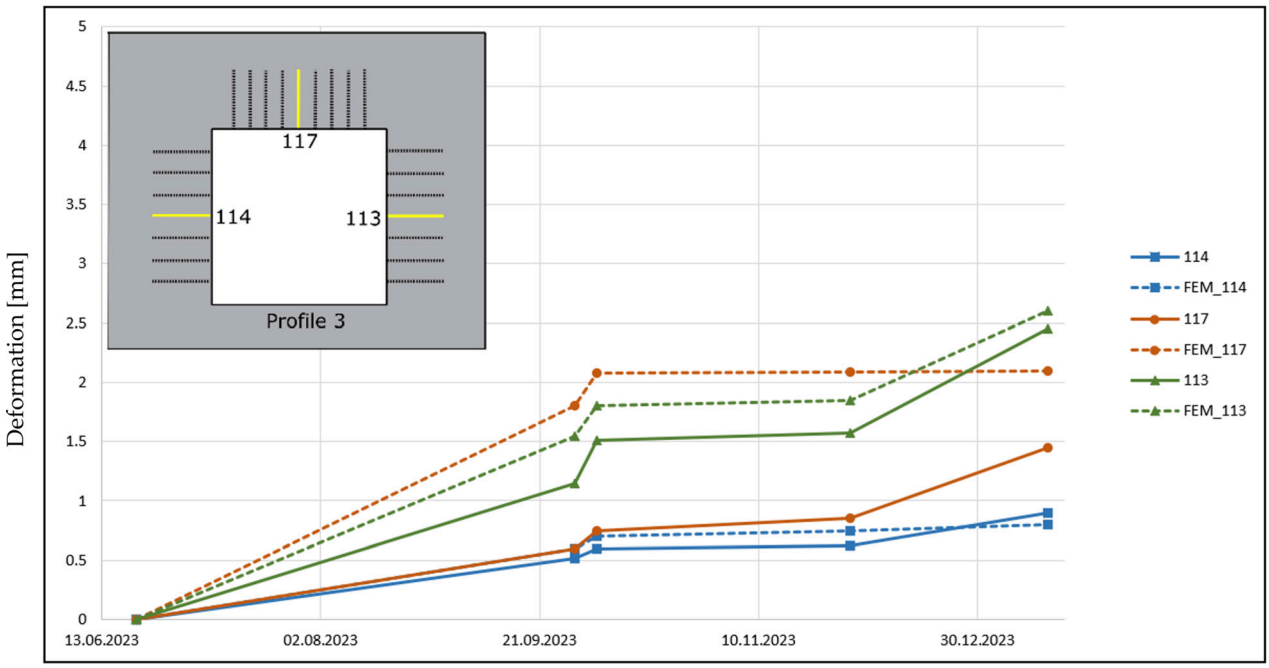


Figure 16. Data comparison: real measurements and simulated data (Profile 3).

Overall, the model successfully captured the general deformation trends observed in the field, including the relative magnitudes and the spatial distribution across the three profiles. The trends in the simulation closely follow those in the measured data, demonstrating that the simplified elastic model is capable of reproducing the essential deformation behaviour.

However, some differences remain, as the model is not fully precise because of the inherent differences between the simplified elastic numerical model and the complex reality. These differences arise from factors such as material heterogeneity and the limitations of the model assumptions.

To address these discrepancies and improve data precision, statistical data analysis techniques were used. Analysing the differences between real and simulated data allows the numerical model to better align with observed field data. The modifications aim to improve the model's accuracy, resulting in more reliable predictions and a better match to real-world behaviour. For the two datasets—the measured deformations and the numerical model predictions—Pearson's correlation coefficient was calculated to assess the strength of their linear relationship. The correlation value was 0.9; while not perfect, it indicates a strong positive correlation between the model deformation and measured deformation data.

4.3.1. Profile 1 Data Comparison

The comparison between measured and simulated deformation for Profile 1 reveals the most challenging fit among the three profiles (Figure 14). At the early stages, discrepancies are notable, particularly due to the previously discussed settlement and delayed installation of the intelligent rock bolts. In reality, some deformation occurred before monitoring began, whereas in the model, the bolts were present from the start of excavation, making it difficult to replicate the initial settlement behaviour precisely.

As deformation progressed, the agreement between measured and modelled results improved. Major excavation events, such as the stoping stage, align more closely between the two datasets, since the timing of these activities was well known and could be directly incorporated into the model sequence.

This profile also contains the observed joint crossing two bolts, which contributed to differences in deformation measurements, especially for the roof bolt. Without precise joint parameters in the model, its localised influence on rock movement could not be perfectly reproduced. Despite these challenges, the model captured the general deformation trend, and the magnitude correlation for major events is satisfactory.

4.3.2. Profile 2 Data Comparison

Profile 2 shows a good correlation between measured and simulated data (Figure 15). Because it is located further from the main stope development and unaffected by the joint present in Profile 1, this profile experienced a more uniform deformation redistribution. The reduced influence of geological anomalies allowed the elastic FEM model to reproduce deformation patterns more consistently.

Differences between simulation and measurement are minor and generally limited to early-stage deformation, which again is partly explained by the bolt installation delay and initial settlement. For subsequent excavation stages, the simulated deformations follow the measured trends closely, both in magnitude and timing.

4.3.3. Profile 3 Data Comparison

Profile 3 shows a good correlation between the measured and simulated deformations (Figure 16). The general trends align well throughout the monitoring period, and the influence of the nearby drift—particularly the increased deformation recorded by bolt 113—is also captured effectively by the model.

The only notable difference occurs in the roof bolt, where the simulated deformation overestimates the measured value. This behaviour is consistent with patterns seen in other profiles and is likely related to the more complex conditions in the roof area and possible small-scale discontinuities in the roof that are not explicitly represented in the model.

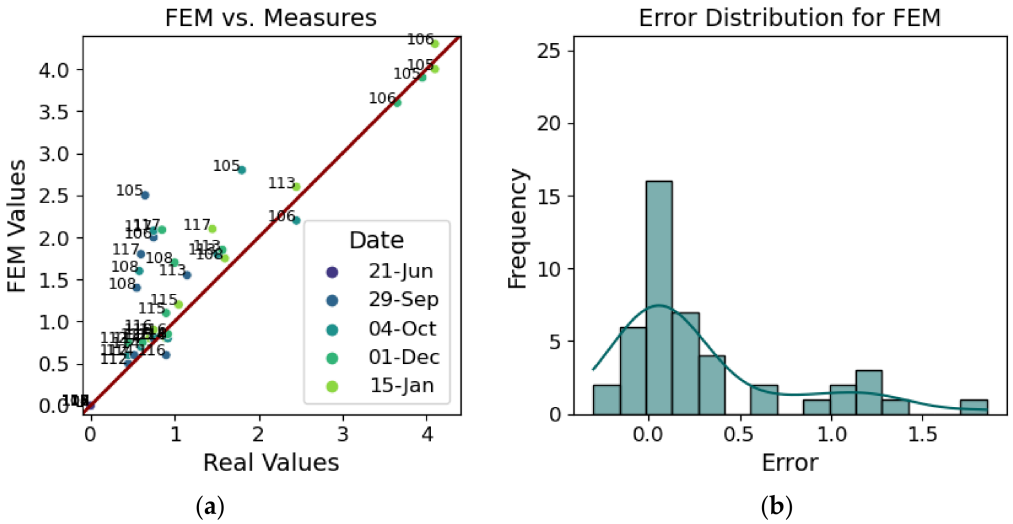
Overall, the match in both magnitude and timing for the remaining bolts demonstrates that the model successfully reproduced the main deformation characteristics of this profile, even in the presence of a local geological influence from the adjacent drift.

4.4. Analysis of FEM Model Result

This section quantifies how closely the FEM model's predicted deformations match field measurements and identifies the systematic error pattern that motivates the statistical correction developed in Section 4.5.

The comparison was performed point by point at matching, event-based time steps (using $n = 45$ paired measurements across all monitored bolts), so that simulated deformations could be checked against field measurements at equivalent stages of mine development. Deformation was used as the validation metric because it could be extracted directly from the model without additional conversion, avoiding an extra source of error. Correlation analysis yielded a strong coefficient ($r = 0.906$, 95% CI 0.834–0.948) between simulated and measured data, confirming that the FEM model reproduces the general deformation trend well. However, the correlation coefficient alone hides a structural problem. Scatter plots.

Figure 17 reveals variations. The FEM overestimates deformations for bolts 105, 117, and 108 by up to 2 mm, with a non-normal, left-skewed error distribution (skewness = −1.48) and a secondary peak that the model fails to capture—consistent with localised fracture-driven movement that a simplified elastic model cannot represent. Although overall patterns align, these significant deviations affect stability assessments, underscoring the need for real-data integration as outlined previously. The data confirm that, despite similar deformation patterns, FEM deviations are substantial for stability analysis and can be mitigated through real-data integration.



(**a**) (**b**)

Figure 17. FEM model deformation result (**a**) and error distributions (**b**).

To refine FEM deviations, there are different methods available; the easiest white box model is regression. Strain-stress curves, which govern deformation behaviour, exhibit significant changes—particularly during transitions to plastic deformation, hardening, and post-cracking [30] —rendering non-linear fitting more adaptable for capturing these nonlinearities (Table 4). Therefore, to correct the numerical simulation, the performance of three models is provided for comparison: classical linear regression, and versions with introduced nonlinearity in exponential and polynomial forms.

Despite the improvement in simulation results, regression adjustment is not designed for dynamic processes such as deformation. The process itself changes over time and requires a dynamic weighting scheme that updates as new data become available. A static regression correction, once fitted, remains fixed regardless of how the deformation process evolves, and cannot distinguish between genuine physical change and measurement noise.

Comparisons show that linear adjustments deliver negligible gains in error distribution or precision, with the original FEM's secondary pattern persisting and curbing the overall impact. Conversely, polynomial and exponential models modestly boost correlation and reduce skewness for more normal errors, which is superior to the baseline models, though residuals persist. These limitations reflect a broader shortcoming of regression-based correction: it treats each measurement independently and provides no mechanism for propagating uncertainty or updating predictions sequentially as monitoring continues.

For a dynamic monitoring context such as this, where field measurements are collected sequentially over the course of mine development, the Kalman filter offers a more suitable framework. Rather than fitting a single static correction, the Kalman filter recursively updates its estimate of the true deformation state at each time step by combining the FEM model's prediction (the process model) with the incoming field measurement, weighting each according to their respective uncertainties. This allows the correction to adapt dynamically as new measurements arrive, converging toward the field-measured trend while smoothing out short-term measurement noise, and explicitly modelling the evolving discrepancy between simulated and real deformation rather than assuming it is constant. For superior integration of measured data, the Kalman filter stands out, as elaborated below.

Table 4. Summary of statistical fitting and post-processing approaches applied to FEM model outputs compared to measured deformations.

	FEM	Linear	Exponential	Polynomial	Kalman Filter
		0.86·FEM−0.11	**$0.38 \cdot e^{0.59 \cdot FEM}$**	**$0.156 \cdot FEM^2$+0.29 FEM+0.18**	
Mean	0.29	−0.007	0.04	0.001	−0.001
Skew	−1.53	−1.05	−0.20	−0.7	1.13
Std	0.49	0.46	0.40	0.39	0.26
Correlation	0.906	0.906	0.92	0.93	0.97

4.5. Implementation of the Kalman Filter for FEM Result Adjustment

In this study, applied to rock deformation monitoring, the filter acts as an adaptive estimator: it predicts subsurface displacements using finite element method (FEM) simulations (based on rock-mechanical properties), then updates these with in situ data from instrumented rock bolts—optimising residuals for progressively refined, probabilistic forecasts during excavation. As a secondary refinement atop polynomial adjustments—which stabilise spatial nonlinearities—the Kalman filter grounds predictions in physical laws while sequentially leveraging bolt measurements for targeted, time-dependent corrections [31].

The basic idea of the Kalman filter is to combine pre-calculated simulation data with sequential sensor measurements to dynamically calibrate deformation predictions. While FEM simulation outputs are known from the beginning of the analysis, sensor data become available iteratively as actual deformation occurs, making model calibration an essential task. Unlike static regression approaches or auxiliary features—which fail to capture evolving dynamic processes—the Kalman filter dynamically weighs each data source based on its relative reliability.

Following a standard state-space representation [29,32], the system dynamics and observation models are structured to capture deformation behaviour over time. First, the state vector is formulated to represent the deformation state and its rate of change (first derivative). This is followed by the state transition matrix (A), which incorporates the time steps, alongside the observation matrix.

The initial weighting between measurements and simulations is governed by the covariance matrices Q and R. Sensor uncertainty (R) is defined statistically based on signal noise (0.0025 mm^2), whereas the process noise covariance matrix (Q) for the FEM model is set to a lower value (10^{-4}) to reflect high confidence in the overall trend of the physical model while retaining flexibility for unmodeled local effects. The sensitivity analysis evaluating the influence of process noise and observation noise variations on the filtering accuracy is provided in Figure 18. Because the error covariance matrix updates dynamically, extended data observation progressively improves the results, with noticeable stabilisation occurring within the initial time steps.

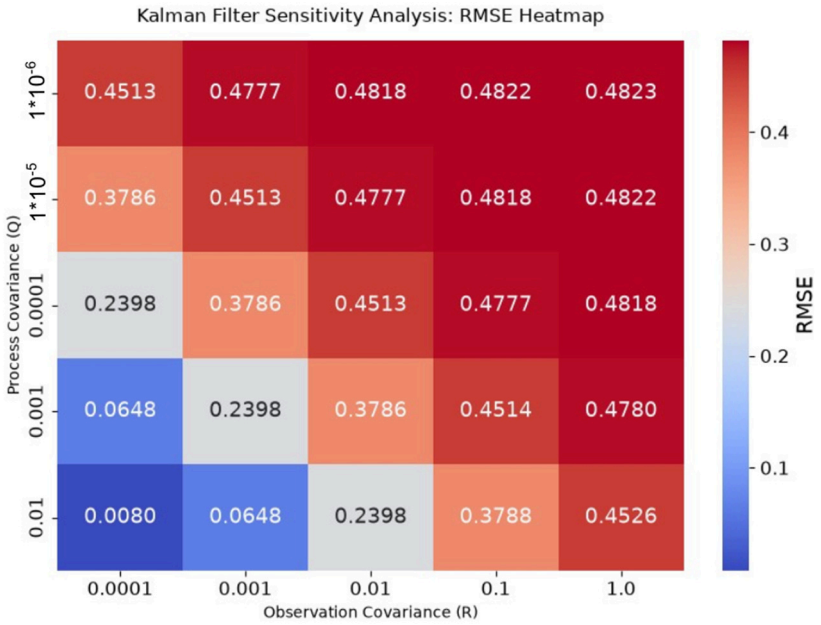


Figure 18. Sensitivity analysis for parameters of R and Q.

In this study, the implementation of the Kalman filter serves as a practical demonstration of real-time data integration for stability analyses driven by sensor measurements. Extending this approach to incorporate spatial dimensions could enable adjustments to stability assessments in the regions between monitoring profiles. However, current data limitations restrict a comprehensive spatial analysis; as the number of dimensions considered increases, the required data volume grows exponentially, presenting a fundamental constraint.

The Kalman filter was implemented using Python libraries [32] on a dataset of 45 time-dependent measurements (ungrouped by location). Performance evaluation (Figure 19) via a boxplot of errors across scenarios (original FEM: "Original Deviation"; polynomial-corrected: "Polynomial Corrected"; Kalman-refined: "Kalman Corrected")—reveals an initial variance inflation from bootstrapping, followed by a progressive reduction: medians converge toward zero (orange line), and box ranges narrow, signifying enhanced precision over time.

Figure 20 illustrates the error distributions, revealing substantial improvements following Kalman refinement. Original FEM errors exhibit a mean of 0.29 mm (std: 0.26 mm) against an average deformation of 1.04 mm, yielding ~28% relative error and non-normal tails due to high skewness. Advanced corrections via rock bolt data shift the mean to −0.001 mm (std: 0.26 mm), halving uncertainty and enhancing FEM accuracy. Thus, the Kalman filter integration post-regression approximately doubles FEM prediction precision, reducing the root mean square error (RMSE) by ~54% (from 0.49 mm std to 0.26 mm, equating to a 3σ confidence bound shrinking from ~1.44 mm to ~0.78 mm). This enhanced accuracy enables proactive detection of instability thresholds in mine excavations, mitigating risks of rockfalls or collapses, thereby bolstering operational safety and informing timely reinforcement strategies for underground structures.

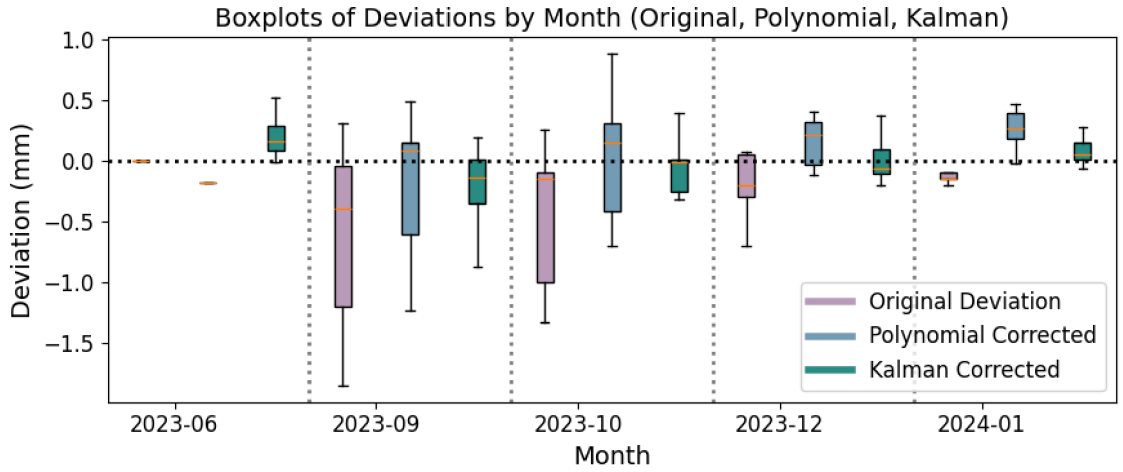


Figure 19. The temporally grouped deviation of FEM results, polynomial adjustment, and corrected by the Kalman filter.

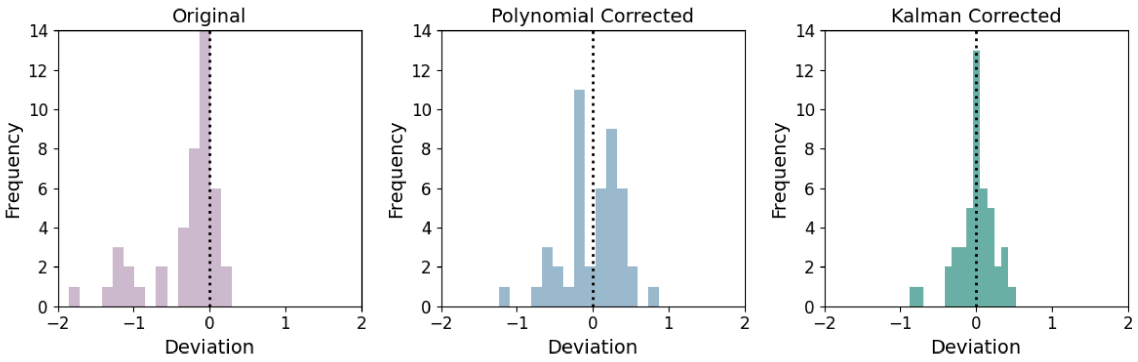


Figure 20. Deviation distributions.

5. Conclusions

Mining digitalisation continues to improve the safety, productivity, and sustainability of underground mining, with intelligent rock bolts representing one of the emerging technologies supporting this transition. This study presented a methodology for integrating intelligent rock bolt measurements with numerical modelling for model validation and demonstrated the feasibility of this approach.

The results showed that intelligent rock bolts provided reliable and consistent deformation measurements that agreed well with the numerical model in both deformation magnitude and overall trends. A strong correlation between simulated and measured deformation confirmed that intelligent rock bolt data can be successfully used for the empirical validation of numerical models. Furthermore, statistical post-processing methods, particularly polynomial correction and the Kalman filter, further improved the agreement between numerical predictions and field measurements.

The proposed methodology provides a practical framework for integrating real-time monitoring data into numerical simulations, enabling iterative model refinement and supporting a more reliable ground behaviour assessment. This demonstrates the potential of intelligent rock bolts to contribute to safer and more efficient underground mining operations.

Future work should focus on improving spatial monitoring density, installing intelligent rock bolts immediately after excavation to capture the complete deformation history, incorporating more detailed geological information into numerical models, and investigating more advanced modelling approaches capable of representing rock mass

discontinuities. These developments are expected to further improve model accuracy and broaden the applicability of the proposed methodology.

6. Limitations

The methodology presented in this study offers a practical and reproducible approach for validating numerical models with field measurements, but certain limitations should be considered to contextualise the results. Only a limited number of intelligent rock bolts were installed due to logistical and cost constraints, meaning that the measurements may not capture the full spatial variability of rock mass behaviour across the monitored section. The spatial resolution of the reconstructed deformation field is inherently dependent on the density and distribution of intelligent rock bolts. The present study evaluated the proposed correction methodology using the available monitoring layout and did not investigate the influence of alternative sensor spacing. Consequently, local deformation variations occurring between monitoring locations may remain undetected. Future work should investigate the optimal sensor density through dedicated numerical sensitivity analyses and statistical simulations.

The simulations assumed an elastic, homogeneous, competent hard rock mass due to the absence of a detailed geological model. This simplification reduced the number of required input parameters, enabling the modelling to be performed on a standard laptop and making the methodology computationally efficient and easily reproducible. While the model provides useful insights into general stress and deformation patterns, it does not fully capture localised responses or failure mechanisms controlled by the inherent heterogeneity of the rock mass. The proposed methodology was developed and validated for relatively stable deformation conditions in a hard-rock underground mine. Applications involving rapidly changing deformation, strong dynamic loading, or rock burst-prone environments may require higher measurement frequencies and different filtering strategies. These conditions were outside the scope of the present study and should be investigated in future work.

Model validation relied on correlations of 85–98% and was limited by the small daily deformations (<1 mm/day) characteristic of the monitored site. Local heterogeneities, such as cracks and variations in material properties, can produce differences even over short distances, making the validation inherently indirect. Because the individual error sources act simultaneously, their respective contributions cannot be isolated within the framework of the present study.

While the present study relies solely on intelligent rock bolt measurements, the multi-sensor approach proposed by Schild et al. demonstrates how combining complementary monitoring systems may reduce some of the limitations associated with sparse spatial measurements and geological uncertainty. The dataset used for Kalman filtering focused solely on temporal dependencies due to the limited number of installed rock bolts during the monitoring period and the constraints of short-term monitoring relative to long-term failure mechanisms. Furthermore, the exponential increase in data requirements explains the limitations of multi-dimensional spatial analysis. Future work could incorporate spatial integration and neighbouring-point constraints to provide a more comprehensive understanding of rock mass behaviour. Finite element method (FEM) deviations of up to 2 mm persist due to uncaptured fractures and nonlinearities, while the Kalman filter assumes Gaussian noise and may underperform under non-stationary dynamics or with larger datasets. These limitations could be addressed in future studies through multi-sensor fusion and larger-scale validations [33].

Finally, the study is based on short-term monitoring, which may not fully reflect long-term rock mass responses under varying mining conditions or across different rock

masses (e.g., soft rock or deep mining). Despite these considerations, the methodology provides meaningful insights into rock mass behaviour and offers a balance between practical applicability, reproducibility, and computational efficiency, making it a useful approach for real-world mining scenarios.

Author Contributions: M.V.: Conceptualisation, Data curation, Formal analysis, Investigation, Methodology, Validation, Visualisation, Writing—original draft. A.B. (Aleksandra Babaryka): Formal analysis, Validation, Visualisation, Writing—original draft. K.F.: Investigation, Resources, Writing—original draft. A.B. (Aleksandra Bondarchuk): Investigation, Resources, Writing—original draft. P.H.: Conceptualisation, Funding acquisition, Project administration, Supervision, Writing—review and editing. All authors have read and agreed to the published version of the manuscript.

Funding: This paper was prepared within the framework of the illuMINEation project. The project has received funding from the European Union's Horizon 2020 research and innovation program under grant agreement No. 869379.

Data Availability Statement: The data that support the findings of this study are available from the corresponding author upon reasonable request.

Acknowledgments: We are grateful for the Boliden company team's dedication to collecting data, sampling boreholes, and installing intelligent rock bolts. Special thanks to K. Ungerer for additional comments regarding the work and support. During the preparation of this work, the author(s) used chat.gpt and Grammarly software to improve grammar, readability and text clarity. After using this tool/service, the author(s) reviewed and edited the content as needed and take(s) full responsibility for the content of the published article.

Conflicts of Interest: Author Krzysztof Fulawka was employed by the company KGHM CUPRUM Ltd. Author Alexander Bondarchuk was employed by the company Boliden AB. The remaining authors declare that the research was conducted in the absence of any commercial or financial relationships that could be construed as a potential conflict of interest.

References

1. Eurostat. *Incidence Rate of Non-Fatal Accidents at Work, EU, 2012–2021*; European Union: Brussels, Belgium, 2024. Available online: https://ec.europa.eu/eurostat/statistics-explained/index.php?title=Accidents_at_work_-_statistics_by_economic_activity (accessed on 8 December 2025).
2. Duzgun, H.S.B.; Einstein, H.H. Assessment and management of roof fall risks in underground coal mines. *Saf. Sci.* **2004**, *42*, 23–41. [CrossRef]
3. Stolecki, L.; Grzebyk, W. The velocity of roof deflection as an indicator of underground workings stability—Case study from polish deep copper mines. *Int. J. Rock Mech. Min. Sci.* **2021**, *143*, 104717. [CrossRef]
4. Stolecki, L.; Szczerbiński, K. Practical Use of Measuring the Deflection of Roof Layers in the Assessment of the Stability of Mining Excavations in the Polish Copper Ore Mine "Polkowice-Sieroszowice". *Mining* **2021**, *2*, 13–31. [CrossRef]
5. Varelija, M.; Hartlieb, P. Designing Intelligent Rock Support Systems to Detect Gravity-Driven Wedges. *Rock Mech. Rock Eng.* **2024**, *58*, 4527–4541. [CrossRef]
6. Li, F.; Kong, D.; Li, Q.; Shang, Y.; Cheng, Z.; He, L. Failure analysis and prediction of roof instability in end face under repeated mining using early warning system. *Sci. Rep.* **2023**, *13*, 8764. [CrossRef] [PubMed]
7. Małkowski, P.; Juszyński, D. Roof fall hazard assessment with the use of artificial neural network. *Int. J. Rock Mech. Min. Sci.* **2021**, *143*, 104701. [CrossRef]
8. Wojtecki, Ł.; Iwaszenko, S.; Apel, D.B. An attempt to use machine learning algorithms to predict strong tremors during longwall mining of a coal seam. *J. Appl. Geophys.* **2023**, *218*, 105210. [CrossRef]
9. Brinkgreve, R. *Validating Numerical Modelling in Geotechnical Engineering*; NAFEMS: Knutsford, UK, 2013.
10. Song, G.; Li, W.; Wang, B.; Ho, S.C.M. A Review of Rock Bolt Monitoring Using Smart Sensors. *Sensors* **2017**, *17*, 776. [CrossRef] [PubMed]
11. Di, H.; Xin, Y.; Jian, J. Review of optical fiber sensors for deformation measurement. *Optik* **2018**, *168*, 703–713. [CrossRef]
12. Ho, S.C.M.; Li, W.; Wang, B.; Song, G. A load measuring anchor plate for rock bolt using fiber optic sensor. *Smart Mater. Struct.* **2017**, *26*, 57003. [CrossRef]

13. Pytel, W.; Mertuszka, P.; Fuławka, K.; Lurka, A.; Pałac-Walko, B. Resultant axial stresses in instrumented rockbolts induced by dynamic effects occurred due to multi-face blasting in the working areas. *Tunn. Undergr. Space Technol.* **2021**, *116*, 104088. [CrossRef]
14. Huang, Z.; Tu, Y.; Meng, S.; Bagge, N.; Nilimaa, J.; Blanksvärd, T. Validation of a numerical method for predicting shear deformation of reinforced concrete beams. *Eng. Struct.* **2019**, *197*, 109367. [CrossRef]
15. Singh, P.; Jang, H.; Spearing, A. Improving the Numerical Modelling of In-Situ Rock Bolts Using Axial and Bending Strain Data from Instrumented Bolts. *Geotech. Geol. Eng.* **2022**, *40*, 2631–2655. [CrossRef]
16. Baranowski, P.; Kucewicz, M.; Janiszewski, J. JH-2 constitutive model of sandstone for dynamic problems. *Sci. Rep.* **2024**, *14*, 3339. [CrossRef] [PubMed]
17. Baranowski, P.; Kucewicz, M.; Pytlik, M.; Małachowski, J. Shock-induced fracture of dolomite rock in small-scale blast tests. *J. Rock Mech. Geotech. Eng.* **2022**, *14*, 1823–1835. [CrossRef]
18. Kucewicz, M.; Baranowski, P.; Mazurkiewicz, Ł.; Małachowski, J. Comparison of selected blasting constitutive models for reproducing the dynamic fragmentation of rock. *Int. J. Impact Eng.* **2023**, *173*, 104484. [CrossRef]
19. Adach-Pawelus, K.; Pawelus, D. Influence of Driving Direction on the Stability of a Group of Headings Located in a Field of High Horizontal Stresses in the Polish Underground Copper Mines. *Energies* **2021**, *14*, 5955. [CrossRef]
20. Adach-Pawelus, K.; Szyry, N. Influence of a Type of Rock Mass on the Stability of Headings in Polish Underground Copper Mines Based on Boundary Element Method. *Energies* **2022**, *15*, 5837. [CrossRef]
21. Lasocki, S.; Orlecka-Sikora, B.; Mutke, G.; Pytel, W.; Rudziński, Ł.; Markowski, P.; Piasecki, P. A catastrophic event in Rudna copper-ore mine in Poland on 29 November, 2016: What, how and why. In *Proceedings of the 9th International Symposium on Rockbursts and Seismicity in Mines (RaSiM9), Santiago, Chile, 15–17 November 2017*; Vallejos, J.A., Ed.; Editec S.A.: Santiago, Chile, 2017; pp. 316–324.
22. Fuławka, K.; Stolecki, L.; Jaśkiewicz-Proć, I.; Kołodziej, R. The Use of Large-Scale 3D Numerical Modeling to Identify Areas of Increased Seismic Risk in Polish Underground Copper Mines. In *7th International Conference on Geotechnical and Geophysical Site Characterization*; CIMNE: Barcelona, Spain, 2024.
23. Rincon, J.; Jansson, N.; Thomas, H.; Kaiser, M.C.; Persson, M.F.; Nordfeldt, E.; Wanhainen, C. Ore Remobilization History of the Metamorphosed Rävliden North Volcanogenic Massive Sulfide Deposit, Skellefte District, Sweden. *Econ. Geol.* **2024**, *119*, 907–934. [CrossRef]
24. Geological Survey of Sweden. Ores and Minerals—Geological Data. 2025. Available online: https://apps.sgu.se/kartvisare/kartvisare-malm-mineral.html# (accessed on 8 December 2025).
25. Nöger, M.; Varelija, M.; Hartlieb, P.; Paterek, M.; Kobylanska, M.; Pikuła, M.; Bursa, B.; Rody, M.; Mosberger, R. *D4.4 The Safe Zone Concept. Improved Safety and Environmental Performance*; Project Deliverable—IluMINEation—Horizon 2020; University of Leoben: Leoben, Austria, 2023.
26. Varelija, M.; Nöger, M.; Hartlieb, F.; Dendl, D.; Moser, P. The effect of different rock mass properties on deformation distribution detected with intelligent rock bolts in underground mining. In Proceedings of the 15th International ISRM Congress 2023 & 72nd Geomechanics Colloquium, Salzburg, Austria, 9–14 October 2023.
27. illuMINEation Project Consortium. Bright Concepts for a Safe & Sustainable Digital Mining Future. 2023. Available online: https://www.illumineation-h2020.eu/our-team/consortium-/-partners (accessed on 16 September 2024).
28. Rocscience Inc. RS3 Software. 3D Finite Element Analysis Software. Available online: https://www.rocscience.com/software/rs3 (accessed on 9 September 2024).
29. Welch, G.; Bishop, G. *Introduction to the Kalman Filter (TR 95-041)*; University of North Carolina, Department of Computer Science: Chapel Hill, NC, USA, 2006.
30. Li, T.; Zheng, J.; Chen, Z. Description of full-range strain hardening behavior of steels. *SpringerPlus* **2016**, *5*, 1316. [CrossRef] [PubMed]
31. Murakami, A.; Fujisawa, K.; Shuku, T. Developments of inverse analysis by Kalman filters and Bayesian methods applied to geotechnical engineering. *Proc. Jpn. Acad. Ser. B Phys. Biol. Sci.* **2023**, *99*, 352–388. [CrossRef] [PubMed]
32. Labbe, R. FilterPy: Kalman Filtering and Optimal Estimation Library in Python. 2020. Available online: https://github.com/rlabbe/filterpy (accessed on 23 September 2024).
33. Schild, L.; Scheiber, T.; Snook, P.; Arghandeh, R.; Samnøy, S.F.; Maschler, A.; Kristensen, L. Multimodal Asynchronous Kalman Filter for monitoring unstable rock slopes. *Geomat. Nat. Hazards Risk* **2023**, *14*, 2272575. [CrossRef]

Disclaimer/Publisher's Note: The statements, opinions and data contained in all publications are solely those of the individual author(s) and contributor(s) and not of MDPI and/or the editor(s). MDPI and/or the editor(s) disclaim responsibility for any injury to people or property resulting from any ideas, methods, instructions or products referred to in the content.